PHYS2041 Lab Report
Photoelectric Effect of Visible Wavelengths

Ryan White
s4499039

9th of October, 2020

Abstract

With a traditional current measurement apparatus, the photoelectric effect was observed for one ultraviolet and multiple visible wavelengths of light. With the data obtained, Planck's constant, h, and the work function, ϕ, of the capacitor used were calculated, and conclusions as to the quantum model of light were made. As well as this, the maximum kinetic energies of violet, blue, green, and yellow wavelength photoelectron energy distributions were found together with the relative spread of energies against voltage. The Current-Voltage Characteristic Curve for each wavelength was plotted and used to find the aforementioned photoelectron energy distributions using the two-point forward-difference differentiation formula.

1 Introduction

The photoelectric effect, first discovered by Heinrich Hertz, paved the way for the field of quantum mechanics [2]. With an experimental setup consisting of an elemental lamp, a vacuum tube, a capacitor, and a circuit, the photoelectric effect is observable and measurable with a change in current and voltage as dependent variables. Quantifying the implications of this phenomenon provides crucial insight into the inner workings of quantum mechanics, and allows for the formulation of fundamental physical concepts that a number of technologies and applications rely on.

2 Theory

Under the influence of sufficiently energetic light, electrons on the surface of a metallic substance have been found to break from its parent atom and induce a current in circuit [2]. These electrons, named photoelectrons, are the result of the quantum model of light and constitute a distribution of kinetic energies once ejected, where the resultant current becomes horizontally asymptotic with sufficiently high applied voltage. The value at some voltage of the current-voltage curve of the photoelectrons, $i(V, \nu)$, is the result of the voltage-dependent decaying photoelectron energy distribution function, $N(K, \nu)$. The Photoelectron energy distribution (PEED) is found by the derivative of the current-voltage characteristic curve (CVCC) [1], and so experimentally finding the CVCC allows for the calculation of the PEED via numerical differentiation.

Sauer (2018) describes the approximate numerical calculation of a derivative of some formula with the two-point forward-difference formula:

$$f'(x) \approx \frac{f(x+h) - f(x)}{h} \tag{1}$$

In section 5.1.2 of the same text, Sauer describes that for double-precision calculations, a h value of approximately $h = 10^{-5}$ usually yields the best results, minimising rounding error as a result of numerical calculation.

The CVCC is inherently dependent upon the voltage at which photoelectrons begin to flow through the circuit, denoted the minimum energy E_0, or the work function of the parent metal [2]. Equation (2), from the Laboratory Notes, describes the relationship between stopping potential $V_{\text{cut-off}}$, spatial frequency, and work function ϕ.

$$eV_{\text{cut-off}} = \frac{hc}{2\pi}k - e\phi \tag{2}$$

$$V_{\text{cut-off}} = \frac{hc}{2\pi e}k - \phi \tag{3}$$

Equation (3) gives a linear relationship between $V_{\text{cut-off}}$ and the spatial frequency k, where the gradient, m_{vk}, is the constant $hc/2\pi e$, and the work function is the linear trendline's intercept.

$$m_{vk} = \frac{hc}{2\pi e} \tag{4}$$

3 Experiment

The basic design of a setup capable of observing and measuring the photoelectric effect is shown in Figure 1.

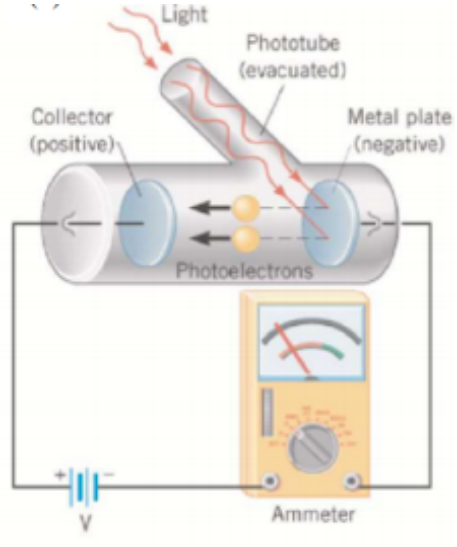

Figure 1: Basic Design of Photoelectric Effect Apparatus

The diagram shows the incident light entering the phototube through a wavelength filter of some aperture width, where the light then strikes an anode, separating photoelectrons that flow towards the cathode and induce a current. The voltage of the circuit is free to be changed (independent variable of the experiment), and directly affects the resultant current measured via the ammeter.

Source: PHYS2041 Laboratory Notes

Unseen in Figure 1 is the mercury lamp situated across from the phototube aperture, and the filter fitted onto the phototube opening.

3.1 Method

Firstly, the mercury lamp was turned on and left for 10 minutes until at appropriate power. The ammeter was then calibrated to read 0A by turning the calibration dial until the readout displayed a value of 0. Following this, the red and black wires were plugged into the apparatus to create the necessary circuit. Starting with the ultraviolet filter (365nm) with an aperture width of 2mm, the voltage dial was rotated until the current value again read 0A. The value of the corresponding voltage was recorded, and the measurement process repeated another 2 times to total 3 separate trials. Following this, the aperture setting was rotated to the 4mm dial, and 3 trials were repeated. Lastly, the aperture width dial was rotated to the 8mm setting, and 3 trials were measured. This process was repeated for the remaining filters of violet (405nm), blue (436nm),

green (546nm), and yellow (577nm).

For the second part of the experiment, the apparatus was calibrated to read 0A and 0V by turning the calibration dials. The mercury lamp was then switched on and allowed to warm up for 20 minutes. The yellow (577nm) filter was then fitted on to the end of the phototube, and the voltmeter dial rotated until -3.2V was displayed. The resultant amperage was recorded, and the voltage increased by 0.1V to -3.1V. This process was repeated until a final voltage of +4V, and the consequent amperage, were recorded. The filter was then swapped to green (546nm) and the measurements taken again. This was repeated for the remaining blue (436nm) and violet (405nm) filters.

3.2 Uncertainties

While every experiment is subject to inherent uncertainties, this investigation presented relatively minimal error. Due to the strictly electronic measurements in the method, the uncertainties were that of the smallest digit on the electronic display. In the case of the ammeter, this corresponded to $\Delta I = \pm 1$A for the majority of measurements. However, as voltage got progressively higher, the amperage was seen to fluctuate over time between a range of values (for constant voltage). In these cases, the uncertainty was deemed to be the difference in the limits from some center point in the fluctuations. Since the voltage was an independent variable, however, the uncertainty remained a constant $\Delta V = \pm 0.1$V across the measurements. As the filters and apertures were supplied without quoted uncertainties in wavelength and width respectively, the error was assumed to be negligible, at least in comparison with that of the ammeter and voltmeter.

4 Results

The results obtained from the first part of the experiment are tabulated in Table 1.

Aperture Width (mm)	Filter Wavelength (nm)	Stopping Potential (V)			
		Trial 1	Trial 2	Trial 3	Average
2	365	-1.99	-1.98	-1.98	-1.98
4	365	-2.01	-2.01	-2.02	-2.01
8	365	-1.94	-1.94	-1.94	-1.94
2	405	-1.53	-1.54	-1.52	-1.53
4	405	-1.55	-1.54	-1.53	-1.54
8	405	-1.54	-1.53	-1.53	-1.53
2	436	-1.33	-1.31	-1.31	-1.32
4	436	-1.32	-1.31	-1.3	-1.31
8	436	-1.3	-1.3	-1.29	-1.3
2	546	-0.78	-0.78	-0.77	-0.78
4	546	-0.79	-0.78	-0.78	-0.78
8	546	-0.77	-0.77	-0.77	-0.77
2	577	-0.69	-0.67	-0.67	-0.68
4	577	-0.67	-0.67	-0.67	-0.67
8	577	-0.65	-0.66	-0.65	-0.65

Table 1: Measured Stopping Voltages for Varying Aperture Widths and Filter Wavelengths

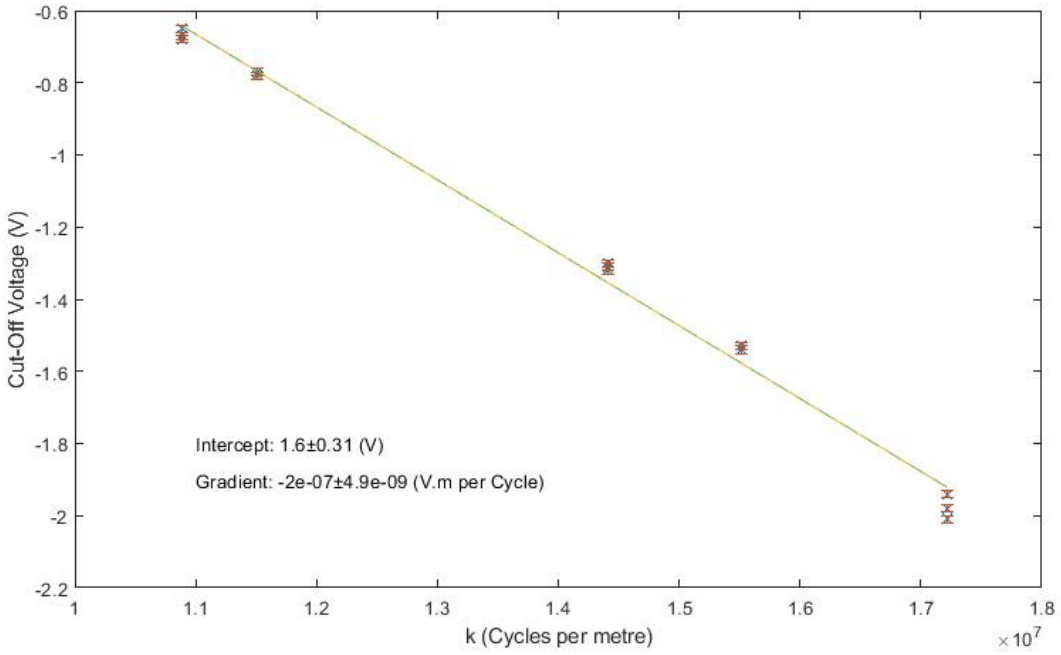

Figure 2: Linear Fit of Cut-Off Voltage vs Spatial Frequency

Figure 2 shows the relationship between Cut-Off Voltage and Spatial frequency, with a linear trendline of the approx $-2.02 \pm 0.049 \times 10^{-7}$ Volt-Meters per Cycle. From equation (4), Planck's constant h may be calculated using known values of the remaining constants.

$$\begin{aligned} m_{vk} &= \frac{hc}{2\pi e} \\ h &= \frac{2\pi me}{c} \\ &= \frac{2\pi \times -2.02 \times 10^{-7}\,(\text{V.m per Cycle}) \times -1.602 \times 10^{-19}(\text{C})}{299792458\,(\text{m/s})} \\ &\approx 6.78 \pm 0.16 \times 10^{-34}\,\text{J.s}^{-1} \end{aligned}$$

Where the uncertainty, $\Delta h = \pm 0.16 \times 10^{-34}$ J.s^{-1}, was calculated in Appendix 7.2. Since equation (3) is of the form of a linear line, represented by Figure 2, the work function represents the y-intercept on the graph, seen as $\phi = 1.56 \pm 0.31$ Volts.
As Table 1 shows, there is some variation in Stopping Voltage against the aperture width of the phototube. Figure 3 visualises this, with separate trendlines in terms of incident wavelength.

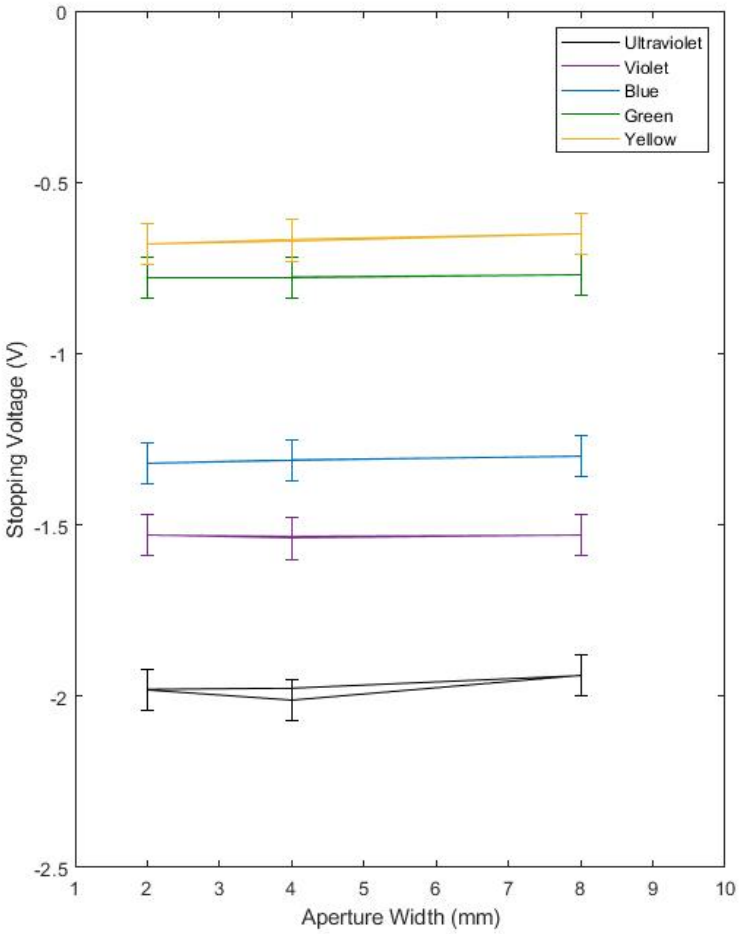

Figure 3: Stopping Voltage vs Aperture for Different Incident Wavelengths

Wavelengths analysed were 365nm, 405nm, 436nm, 546nm, and 577nm for Ultraviolet, Violet, Blue, Green, and Yellow respectively. The linear trendlines clearly fit within the uncertainty of $\Delta V = \pm 0.06$V, and are consistently positive in gradient, indicating that stopping voltage increases as aperture width widens, although only very slightly.

Assuming that a larger aperture equates to a higher light intensity, Figure 3 suggests that greater light intensity correlates with a higher stopping potential. However, section 2.1 of the laboratory notes states that the maximum kinetic energy of the photoelectrons is independent of incident light intensity, and this relationship suggests that light intensity only alters the distribution of the photoelectron kinetic energies, rather than it's peak.

Appendix 7.3 shows the data for the second part of the experiment; measuring the induced current from an independent voltage. Figure 4 graphically represents this data, with partitions in terms of incident wavelength.

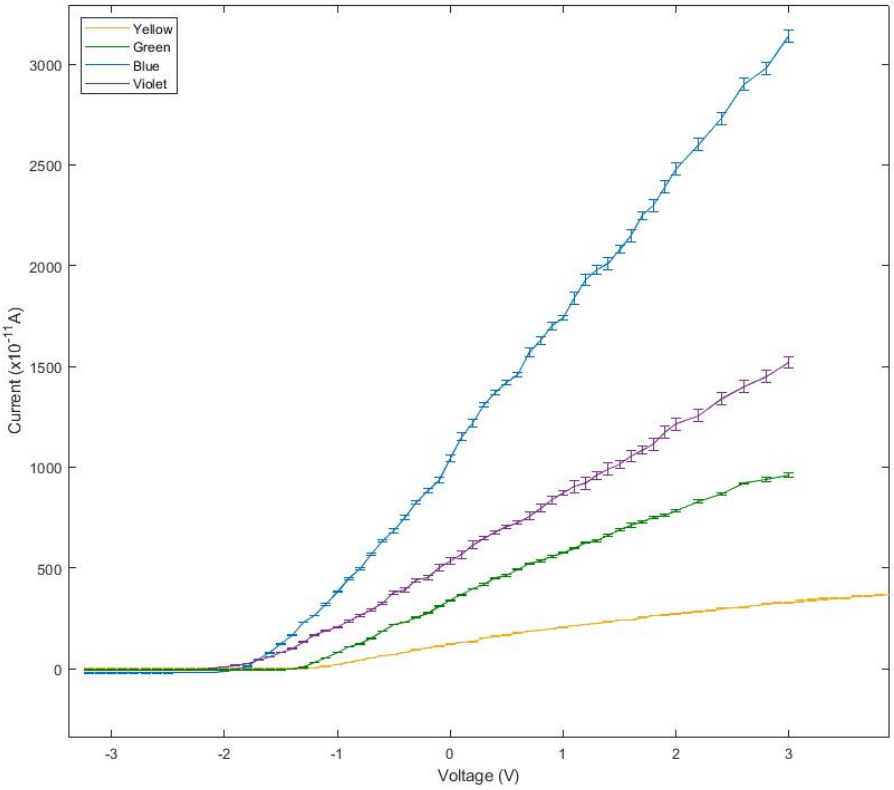

Figure 4: Induced Current vs Voltage for Photoelectrons

Corresponding wavelengths to colours displayed were approximately 577nm, 546nm, 436nm, and 405nm for the yellow, green, blue, and violet curves respectively. A smaller domain of data was available for the non-yellow curves as a result of time constraints. Uncertainties were heavily dependent on the magnitude of the current, and so a higher induced current suffered an inherent greater uncertainty.

While Figure 4 clearly shows the magnitude of I-V Characteristic Curves, the relative stopping potentials are more clearly seen in Figure 5.

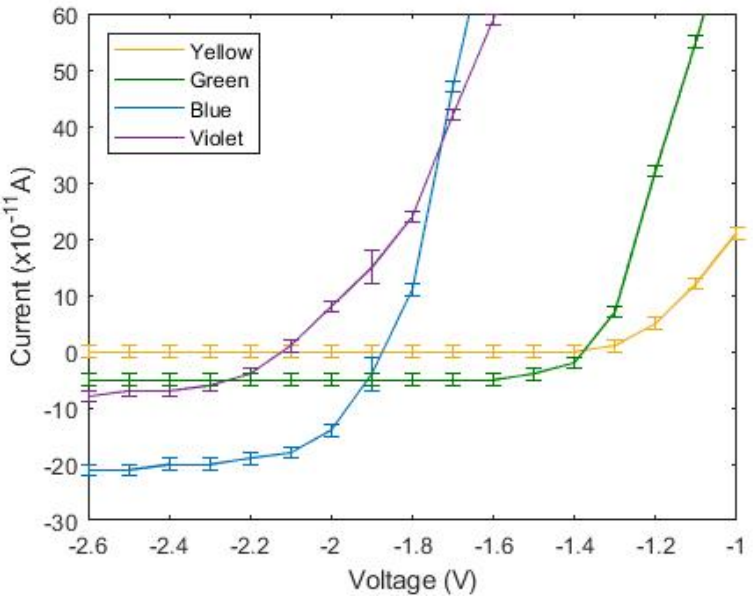

Figure 5: Approximate Stopping Voltages for Varying Incident Wavelengths

Zoomed in snapshot of Figure 4, showing the stopping potentials (first point where $dI/dV \neq 0$) for the different wavelengths of incident light. Approximate values are; Yellow = -1.3V, Green = -1.6V, Blue = -2.5V, Violet = -2.4V. Uncertainties in these values are approx. $\Delta V = \pm 0.1$V.

The data shown here correlates that shown in Figure 3, where a shorter wavelength equates to a more negative stopping potential, bar the data for blue (436nm) in this case. As Figure 6 shows, blue light induces photoelectrons with vastly higher kinetic energies, and so a lesser stopping potential seems to correlate with a high maximum kinetic energy.
The calculated photoelectron energy distribution, the derivative of the Current-Voltage Characteristic Curve (IVCC) of Figure 4, is shown in Figure 6.

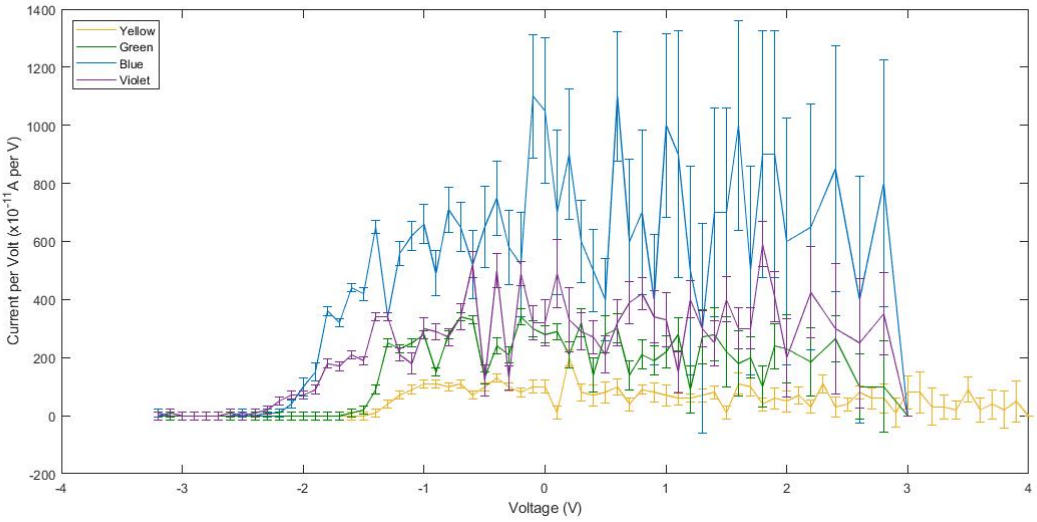

Figure 6: Electron Energy Distribution across Voltage

Colours represented are of the same wavelength as those in Figure 4. Approximate distribution peak kinetic energies were found at: Yellow = (-0.4V, 13×10^{-10}A/V), Green = (-0.7V, 34×10^{-10}A/V), Blue = (-0.1V, 11×10^{-9}A/V), Violet = (-0.6V, 52×10^{-10}A/V).

This shows that, at least in the visible wavelengths tested, blue light of 436nm yields photoelectrons with the greatest kinetic energies, while yellow light of 577nm yields the lowest kinetic energies.

5 Discussion

The Photoelectron Energy Distributions (PEED) shown in Figure 6 seem to resemble a skewed Bell Curve, with a smooth incline in kinetic energy with increasing voltage up to a peak, and then a roughly linear approach to 0 as $V \to \infty$. As the data shows, the green and blue wavelengths in particular were characterised by a sharper ascent to their kinetic energy peak, whereas the other wavelengths showed a more gradual rise. Despite these differences, each PEED was subject to a roughly linear decline as the voltage increased from that at the peak kinetic energy. This claim of linear decline was supported by a series of alternate data shown in Appendix 7.4, where the domain of voltages tested was far greater.

Continuing on from the analysis of Figure 3, Sherrill (2006) explains that, under a wave model of light, a more intense beam of light, and hence one with a larger amplitude, would eject photoelectrons with a larger kinetic energy. This, however, was not observed; there even being weak correlation of the contrary. Instead, this analysis had shown that the kinetic energy distribution, and hence the maximum kinetic energy of the ejecta, depended solely on the wavelength of incident light, with (in the visible spectrum) blue light causing the greatest peak of kinetic energies. As a result, the photoelectric effect is a result of the quantum (or rather, photonic) model of light.

As quoted in the results section, the linear regression fit yielded a work function of $\phi = 1.56 \pm 0.31$ Volts. From Table 38.1 in Knight (2017), this calculated work function was well below the quoted values for typical metals, which quite likely allowed the observation of the photoelectric effect in visible wavelengths (lesser energetic wavelengths than that of ultraviolet wavelengths, typically used to observe the photoelectric effect). Due to this, the detector metal used could be an alloy, a semiconductor, or perhaps one with a significant net negative charge.

6 Conclusions

Using a traditional current measurement apparatus to observe and measure the photoelectric effect, stopping voltages for a range of wavelengths and a subset of varying aperture widths were measured and used to calculate both Planck's constant (within uncertainty) and the work function of the metal anode used in the experimental setup. Using this data, the quantum model of light was enforced due to the light-intensity evidence (Figure 3) conflicting with that which is suggested by *only* the classical wave model of light.

Furthermore, the current-voltage characteristic curve (IVCC) was plotted from obtained measurements (Appendix 7.3) of current, and used to plot the photoelectron energy distribution (PEED) for violet, blue, green, and yellow incident wavelengths of light. With this, it was found that, out of the 4 visible wavelengths tested, blue light of 436nm produces the most energetic photoelectrons, with yellow light of 577nm producing the least energetic. The hypothesized skewed bell curve distribution was supported using large-domain current-voltage measurements (Appendix 7.4.3), where there was an initial steep slope, followed by a gradual (approximately) linear descent following the peak of the distribution.

7 Appendices

7.1 Uncertainty Propagation Table

Relationship	Uncertainty obtained from
General expression	
p = f(x,y,z,...)	$(\Delta p)^2 = \left(\frac{\partial f}{\partial x}\Delta x\right)^2 + \left(\frac{\partial f}{\partial y}\Delta y\right)^2 + \left(\frac{\partial f}{\partial z}\Delta z\right)^2 + \ldots$
Specific cases	
p = x + y	$\Delta p = \sqrt{(\Delta x)^2 + (\Delta y)^2}$
p = x − y	$\Delta p = \sqrt{(\Delta x)^2 + (\Delta y)^2}$
p = x y	$\frac{\Delta p}{\lvert p\rvert} = \sqrt{\left(\frac{\Delta x}{x}\right)^2 + \left(\frac{\Delta y}{y}\right)^2}$
$p = \frac{x}{y}$	$\frac{\Delta p}{\lvert p\rvert} = \sqrt{\left(\frac{\Delta x}{x}\right)^2 + \left(\frac{\Delta y}{y}\right)^2}$
p = Bx	Δp = B Δx
$p = Ax^n$	$\frac{\Delta p}{p} = n\frac{\Delta x}{x}$
p = log x	$\Delta p = \frac{1}{2.3x}\Delta x$
p = sin θ	$\Delta p = \lvert\cos\theta\rvert\,\Delta\theta$

Figure 7: Uncertainty Propagation Table

7.2 Example Uncertainty Propagation

For the equation

$$h = \frac{2\pi me}{c}$$

the uncertainty in h is

$$\begin{aligned}\Delta h &= \frac{2\pi e}{c} \times \Delta m \\ &= \frac{2\pi e}{c} \times 4.9 \times 10^{-}9 \\ &\approx 1.6 \times 10^{-35}\text{J.s}^{-1}\end{aligned}$$

7.3 Current-Voltage Raw Data

Voltage (±0.1 V)	Yellow (577nm) Current ($\times 10^{-11}$A)	Green (546nm) Current ($\times 10^{-11}$A)	Blue (436nm) Current ($\times 10^{-11}$A)	Violet (405nm) Current ($\times 10^{-11}$A)
-3.1	0±1	-5±1	-21±1	-9±1
-3.0	0±1	-5±1	-21±1	-8±1
-2.9	0±1	-5±1	-21±1	-8±1
-2.8	0±1	-5±1	-21±1	-8±1
-2.7	0±1	-5±1	-21±1	-8±1
-3.2	0±1	-5±1	-22±1	-9±1
-2.6	0±1	-5±1	-21±1	-8±1
-2.5	0±1	-5±1	-21±1	-7±1
-2.4	0±1	-5±1	-20±1	-7±1
-2.3	0±1	-5±1	-20±1	-6±1
-2.2	0±1	-5±1	-19±1	-4±1
-2.1	0±1	-5±1	-18±1	1±1
-2.0	0±1	-5±1	-14±1	8±1
-1.9	0±1	-5±1	-4±3	15±1
-1.8	0±1	-5±1	11±1	24±1
-1.7	0±1	-5±1	47±1	42±1
-1.6	0±1	-5±1	79±1	59±1
-1.5	0±1	-4±1	123±1	80±1
-1.4	0±1	-2±1	165±2	99±1
-1.3	1±1	7±1	230±1	133±1
-1.2	5±1	32±1	264±1	167±1
-1.1	12±1	55±1	320±4	188±2
-1.0	21±1	80±1	382±3	206±3
-0.9	32±1	108±1	448±6	236±2
-0.8	43±1	123±1	497±5	265±2
-0.7	53±1	151±1	568±6	292±2
-0.6	64±1	185±1	633±6	326±4
-0.5	71±1	218±1	685±10	378±2
-0.4	81±1	231±2	750±10	390±5
-0.3	94±1	255±2	825±8	440±3
-0.2	104±1	276±2	883±10	453±3
-0.1	112±1	310±2	935±15	502±3
0.0	122±2	340±2	1045±15	534±5
0.1	132±1	368±2	1150±20	566±6
0.2	133±2	397±2	1220±20	615±10
0.3	153±2	418±4	1310±10	648±5
0.4	161±2	450±3	1370±10	677±4
0.5	168±3	464±5	1420±10	704±4
0.6	176±2	492±4	1460±10	725±5
0.7	186±2	522±3	1570±20	757±6
0.8	190±1	536±4	1630±20	796±4
0.9	199±1	557±3	1700±20	838±4
1.0	207±3	576±4	1740±10	872±8
1.1	214±2	598±4	1840±30	905±5
1.2	220±1	626±4	1930±30	920±5
1.3	226±1	635±7	1980±20	960±4
1.4	233±2	662±6	2010±30	990±5
1.5	241±1	690±7	2080±20	1015±6
1.6	242±2	712±10	2150±30	1055±5
1.7	253±3	730±5	2250±20	1085±5
1.8	263±1	750±5	2300±30	1115±5
1.9	267±2	760±5	2390±30	1174±6
2.0	273±3	784±6	2480±30	1215±6
2.1	278±2			
2.2	285±2	830±10	2600±30	1255±12
2.3	288±1			
2.4	299±3	867±6	2730±30	1340±10
2.5	302±2			
2.6	306±1	920±5	2900±30	1400±20
2.7	314±2			
2.8	320±3	940±10	2980±30	1450±10
2.9	326±4			
3.0	327±3	960±12	3140±30	1520±10
3.1	335±5			
3.2	343±5			
3.3	346±4			
3.4	349±1			
3.5	351±3			
3.6	360±3			
3.7	362±3			
3.8	366±4			
3.9	368±5			
4	373±5			

7.4 Alternate I-V Data

The following Appendix provides alternative data to that analysed in the body of the report. As Appendix 7.4.1 shows, there is a far greater range of voltages assessed, although the step between data points is absolutely much larger; this provides insight into how the distributions behave as voltage approaches larger values, although at comparatively less accuracy than that in the body of the report.

7.4.1 Alternate I-V Raw Data

Voltage (V)	Yellow (577nm)		Green (546nm)		Blue (436nm)		Violet (405nm)	
	Current (10^{-11}A)	ΔI	Current (10^{-11}A)	ΔI	Current (10^{-11}A)	ΔI	Current (10^{-11}A)	ΔI
-3.2	0	1	-5	1	-21	1	-9	1
-2.2	0	1	-4	1	-19	1	-5	1
-1.2	8	1	29	1	277	1	162	1
-0.2	99	1	289	1	950	3	474	3
0.8	193	2	525	3	1680	10	820	10
1.8	262	3	727	3	2380	20	1150	10
2.8	327	3	916	2	3110	30	1489	7
3.8	369	2	1062	3	3570	50	1730	10
4.8	380	2	1125	5	3880	60	1910	15
5.8	415	2	1220	5	4380	60	2120	20
6.8	454	2	1350	7	4890	40	2420	20
7.8	486	3	1450	7	5370	60	2620	20
8.8	513	3	1560	20	5710	60	2820	20
9.8	550	5	1660	10	6080	60	3020	20
10.8	578	6	1770	10	6380	130	3150	10
11.8	600	5	1860	10	6740	100	3330	40
12.8	621	9	1920	10	7040	90	3500	30
13.8	648	6	1990	10	7300	80	3620	20
14.8	667	7	2030	10	7520	80	3800	30
15.8	670	5	2090	10	7770	40	3920	20
16.8	685	5	2140	20	8000	100	4040	20
17.8	707	8	2190	10	8350	100	4130	30
18.8	735	5	2250	10	8530	120	4270	30
19.8	753	5	2320	10	8840	100	4400	60
20.8	758	8	2370	10	9000	150	4520	30
21.8	770	8	2420	10	9260	80	4670	50
22.8	783	8	2430	10	9450	150	4780	50
23.8	790	13	2450	10	9650	150	4870	50
24.8	799	6	2520	10	9900	150	5000	40
25.8	822	10	2520	10	10100	150	5160	70
26.8	828	5	2570	10	10300	150	5250	40
27.8	840	5	2600	10	10450	150	5230	40
28.8	843	10	2610	10	10600	150	5370	40
29.8	840	5	2660	10	10650	150	5420	50
30.8	860	13	2680	10	10750	150	5500	50
31.8	874	8	2690	10	11000	150	5580	70

7.4.2 Alternate I-V Characteristic Curve

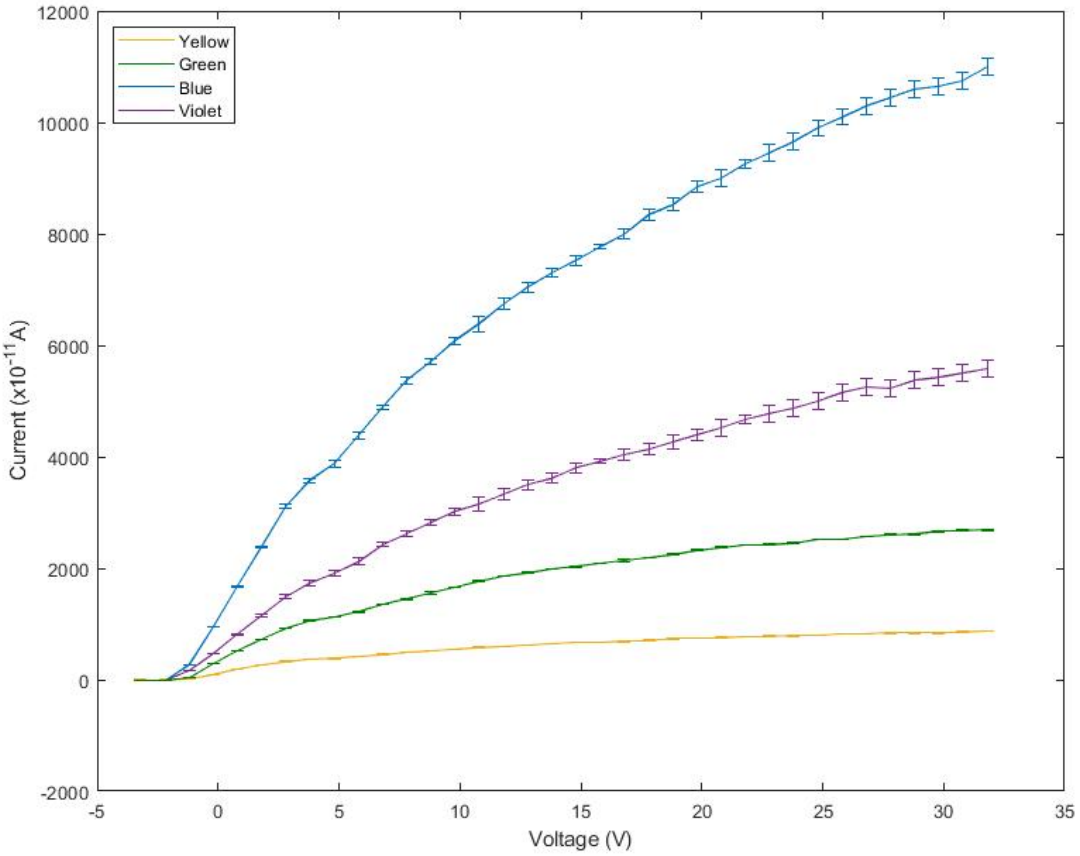

Figure 8: I-V Characteristic Curve over a Greater Domain of Voltage

7.4.3 Alternate Photoelectron Energy Distribution

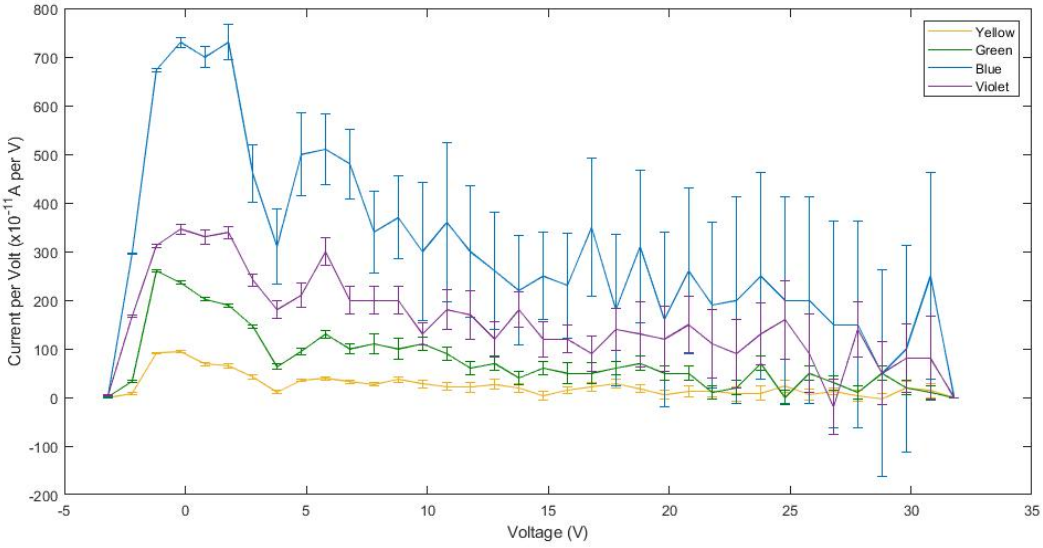

Figure 9: PEED Over a Greater Domain of Voltage

References

[1] Apker, L., Taft, E. & Dickey, J. 1948. *'Photoelectric emission and contact potentials of semiconductors.'* Physical Review, 74 (10), 1462-1474. doi:10.1103/PhysRev.74.1462

[2] Knight, R.D. (2017). '*Physics for scientists and engineers: a strategic approach with modern physics (4th ed.)*'. Boston: Pearson.

[3] Sauer, T. (2018). *'Numerical differentiation and integration. In Numerical analysis'* (3rd ed., pp. 253-292). Hoboken, New Jersey: Pearson

[4] Sherrill, D. (2006). *'The Photoelectric Effect'*. Accessed at <http://vergil.chemistry.gatech.edu/notes/quantrev/node4.html#: :text=According%20to%20the%20classical%20wave,with%20a%20greater%20kinetic%20energy.> on 09/10/2020.